DEBONDING DETECTION IN CF/EP SANDWICH STRUCTURES USING ACTIVE SENSOR NETWORK

S. Mustapha[1], D. Wang[1], L. Ye[1]*
[1] School of Aerospace, Mechanical and Mechatronic Engineering, the University of Sydney, NSW 2006, Australia
Corresponding author: Prof Lin Ye (lin.ye@sydney.edu.au)

Keywords: *Debonding detection, Sandwich structure, Guided waves, Time-reversal*

1 Introduction

A sandwich structure consists of two strong panels separated by a lightweight core such as honeycomb. The separation increases the moment of inertia with a slight increase in weight, producing an efficient structure for resisting bending and buckling loads. It remains a challenge to detect debonding between the surface panel and the core, which may be caused by impact loading or manufacturing defect. Debonding can substantially reduce the performance of sandwich structures.

Structural health monitoring (SHM) techniques based on guided waves propagation have been the subject of interest for researchers since 1980. Guided waves are able to propagate for relatively long distance and have high sensitivity to both surface and embedded structural damage. Accordingly, guided waves have been widely used to develop various damage identification algorithms for assessing delaminations, debonding, holes, cracks/notches and corrosions in both composite and metallic structures [1-3]. Qi et al. [4] have studied the effect of debonding in a composite sandwich structure on the propagation of ultrasonic guided waves. It was demonstrated that guided waves are effective in debonding detection, giving a quantitative estimation of the debonding by calibrating the energy of received wave signals after interacting with the debonding. More work was carried out by Song et al. [5] in an attempt to understand mechanisms of guided wave propagation in composite panels with honeycomb, calculating the wave propagation using finite element models.

2 Aims and Contributions

The aim of this study is to evaluate debonding in sandwich CF/EP composite structures using guided waves and detect debonding using an inverse algorithm based guided wave signals activated and captured by surface-mounted PZT elements. Studies were conducted where debonding of different sizes were introduced at different locations in the composite sandwich structures.

2.1 Experiment set-up

With the PZT actuators and sensors both located on the beam and the plate, Fig.1, activation and acquisition of ultrasonic wave signals were fulfilled using an active signal generation and data acquisition system developed on the VXI platform, consisting mainly of a signal generation unit (Agilent© E1441), signal amplifier (PiezoSys® EPA-104), signal conditioner (Agilent© E3242A) and signal digitizer (Agilent© E1437A). 5-cycle sinusoidal tone bursts enclosed in a Hanning window were generated and applied to the PZT actuator, and the wave signals were captured using the PZT sensor at a sampling rate of 20.48 MHz (A schematic is shown in Fig.2). The acquisition duration was set to insure that at least the first reflected wave signal from the far end of the structure was captured. The structures (sandwich beam or the panel) were simply supported.

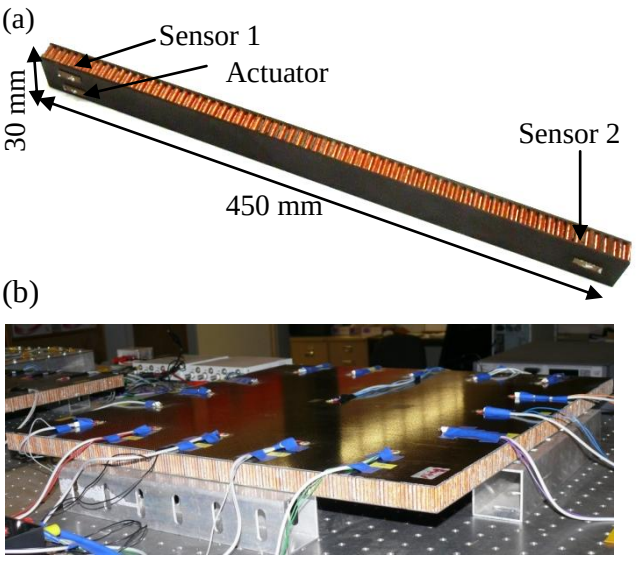

Fig.1: Specimens (a) sandwich beam and (b) sandwich plate

2.2 Debonding in the sandwich CF/EP beams

2.2.1 Specimen preparation

For the sandwich CF/EP composite beams, skin panels were manufactured using Cycom 970/T300 prepregs [3], which consisted of 8 woven plies in a quasi-isotropic lay-up (1.76 mm in thickness). The core was 12.7 mm thick Nomex honeycomb (HRH10-1/8-4) [3]. The specimens were cut into 450 mm (length) × 30 mm (width) sections. Three PZT element electrodes, measuring 20 mm × 5 mm × 1 mm, were surface-mounted on the specimen. One PZT element served as the actuator and the other two served as sensors to capture the incident signal, reflected wave signals (Sensor 1), and transmitted wave signals (Sensor 2) in the composite beams, as shown in Fig.2. One of the specimens was taken as a benchmark without debonding, and debonding of different length was introduced into other specimens by making a cut at the interface between the skin and the core.

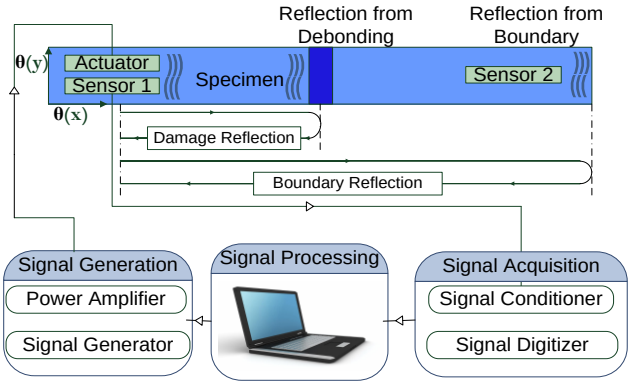

Fig.2: Schematic diagram of experimental set-up

2.2.2 Debonding detection

The fundamental anti-symmetric A_0 mode was activated and captured using the "pulse-echo" configuration. Fig.3 displays the wave signal captured by Sensor 1 in the experiment, activated by the actuator (at 6.5 kHz) in the specimen with debonding of different length at the middle span (x=1/2L). The centre of the debonding was identified from the centre of the actuator and Sensor 1, shown in Fig.2.

$$d = \frac{C_g \Delta T}{2} \quad (1)$$

Where, C_g is the wave propagation velocity in the sandwich beam and ΔT is the difference in ToF (Time-of-flight) between the incident wave signal and the damage reflection captured by Sensor 1.

Further examination was undertaken to evaluate the effectiveness of the A_0 mode in locating debonding in different locations. Debonding of 20 mm in length was placed at the ¾ span (x=3/4L=337.5 mm). The centre of debonding was identified at 328 mm. The evaluation shows the accuracy in detection of debonding in the sandwich CF/EP beam with an error of less than 5%.

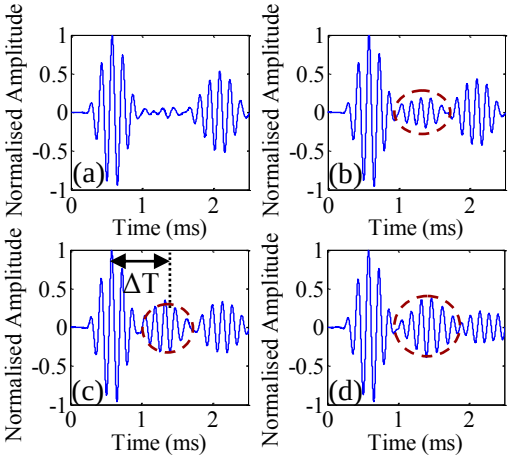

Fig.3: Interaction of waves with debonding of different length: (a) benchmark, (b) 10 mm, (c) 20 mm, and (d) 30 mm

To assess the severity of the debonding, the delays in ToF for both the reflected signals captured by Sensor 1 in a 'pulse and echo' configuration and the transmitted wave signals captured by Sensor 2 in a 'pitch and catch' configuration were evaluated. The length of the debonding was increased gradually, using a thin sharp metal blade, until the entire skin was peeled off the honeycomb core, while the center of the debonding remained the same (at the middle of the span). Fig.4 (a) shows the magnitude of the reflection from the debonding versus the debonding size. As the debonding increased the magnitude of the damage reflected wave increased, but as the debonding was increased beyond 35 mm, the magnitude of the reflection decreased, and began to increase again when the length of debonding reached 70 mm. This phenomenon is attributed to the competition of some influencing factors when the extent of debonding becomes large, (1) the size of damage, which increases the magnitude of the reflection, and (2) the decrease in traveling distance of wave signal, which helps maintain the magnitude of the reflection. In addition, debonding changes the local effective modulus of the structure and, as a consequence, the local speed of the wave varies. When each time the extent of debonding was increased the ToF was determined and the time

delay was calculated relative to the ToF of the beam without debonding. The time delay is plotted against the extent of debonding in Fig.4 (b). The delay in the ToF for both the reflected and transmitted wave signals shows the same trend, noting that for Sensor 1 the delay was halved to account for the fact that the wave is traveling double the distance and it is crossing the debonding twice.

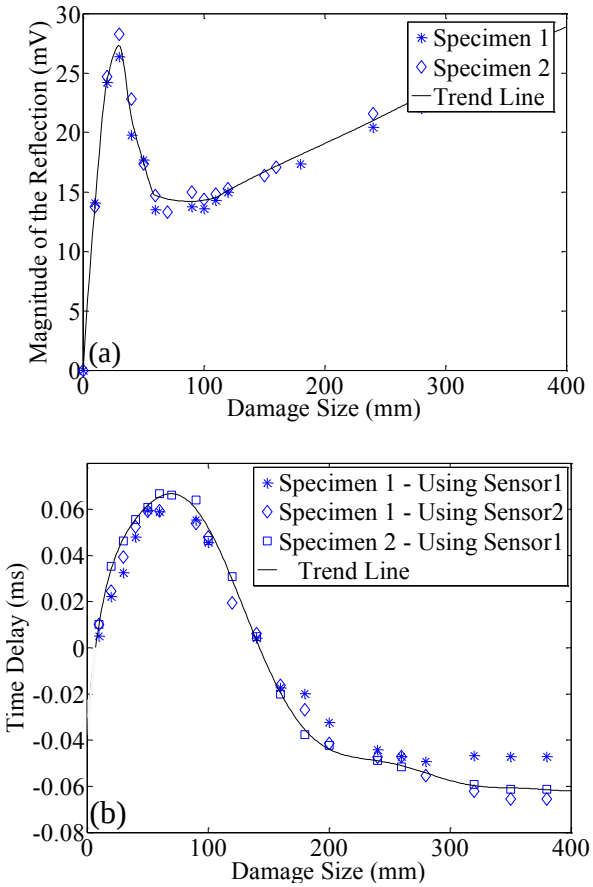

Fig.4: Damage index versus extent of debonding in sandwich CF/EP composite beams (a) magnitude of reflection, and (b) time delay

Furthermore, the time delay initially increased with the increasing extent of debonding. However, as the extent of debonding increased beyond a certain length, the delay began to decrease gradually. This phenomenon is attributed to the fact that the waves propagated in the skin panel when the extent of debonding became large, and the skin panel had a higher effective stiffness than the sandwich beam, allowing the waves to travel more quickly and thus reduce the delay.

2.3 Debonding in sandwich CF/EP plate

An imaging algorithm based on time-reversal wave signals from an active sensor network was developed to detect debonding and damage in composite sandwich panels.

The principle of the time-reversal process in a two-dimensional plate is illustrated in Fig.5, where a tone burst is applied to transducer A functioning as an actuator (step 1), activating a wave signal that is captured by transducer B acting as a sensor (step 2); the captured signal is time-reversed in the time domain (step 3) and reapplied to transducer B that now has an actuating role, then the wave signal at transducer A is collected and time-reversed as a reconstructed signal of the original one (step 4).

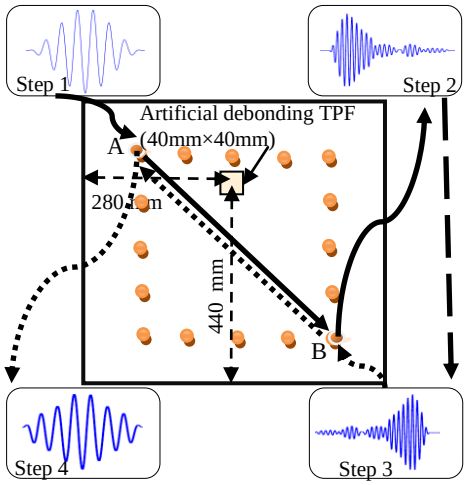

Fig.5: Illustration of the time-reversal process: generation and acquisition of signals

A sensor network was created consisting of sixteen circular PZTs with a distance of 100 mm between elements, enclosing a square area. PZT Elements (P1 to P16) measuring 10 mm in diameter and 1 mm in thickness, were surface-mounted on the sandwich panels. While one PZT element functioned as the actuator to activate wave signals, the others functioned as sensors to capture the wave signals, and the role of actuator alternated until all the PZT elements had functioned as the actuator. The correlation coefficient $\rho_{a,b}(t)$ between the original and reconstructed time-reversal signals was calculated for individual sensing paths in the time domain to get the perception to damage near the sensing paths. The damage index (DI) is defined as:

$$DI = 1 - \rho_{a,b}(t) \qquad (3)$$

For the existence of damage at any location near the wave path, the effect of the DI is confined in a bell shape with a normal distribution function, which means the effect of the DI is maximized on the wave path and decreases gradually as the distance from the wave path increases. Considering a normal

distribution function with mean μ and standard deviation σ, the density function is given by [6]

$$f(z) = \frac{1}{\sigma\sqrt{2\pi}} e^{-\frac{(z-\mu)^2}{2\sigma^2}} \quad \text{For } -\infty < z < \infty \qquad (4)$$

where z was determined using a rectangular affected-zone area for each sensing path by $z = \frac{d}{D_k}$ where d is the normal distance from a node to the kth path and D_k is the distance between the actuator and the sensor of the kth path. The definition of σ was based on an experimental investigation. The monitoring area was meshed into uniform grids and the probability of presence of damage at each grid was estimated by fusion of perceptions to the existence of damage from individual sensing paths. Assuming that there are N sensing paths for damage identification from the sensor network, estimation of the presence of damage at position (x, y) in the monitoring area can be written as [6]:

$$P(x, y) = \sum_{k=1}^{N} DI_k \, f_k(z) \qquad (5)$$

where DI_k and $f_k(z)$ are described in equations (3) and (4) respectively.

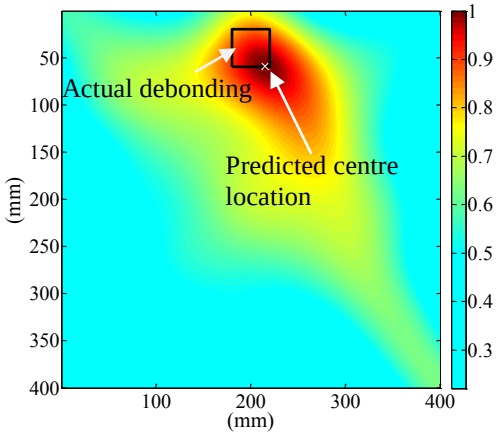

Fig.6: Image construction for locating debonding based on time reversal algorithm

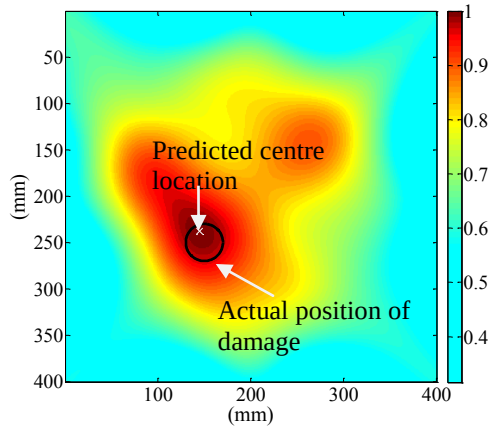

Fig.7: Image construction for locating damage based on time reversal algorithm

This process was applied to each individual path, and P(x, y) at each grid was obtained for the area. The location highlighted by an area with high values of P(x, y) indicates the existence of damage.

Prior to image construction, tuning of the frequency and selection of number of cycles in a toneburst was performed. A frequency of 140 kHz and 7.5 cycles were selected, respectively, to activate the S_0 mode. Wave signals were captured and reconstructed from individual actuator-sensor paths, the original and the reconstructed signals were correlated for each path, and the damage index was defined. Typical images of damage are shown in Fig.6 and Fig.7.

3 Concluding remarks

The use of guided waves for debonding detection in composite sandwich structures was demonstrated. The debonding location and severity of damaged were assessed in sandwich CF/EP beams based on the time of flight and the time delay.

A time-reversal algorithm based on correlation analysis using ultrasonic wave signals from an active sensor network for identifying debonding and other damage in sandwich CF/EP plates was developed. The results highlight that the guided wave signals are good candidates for detecting and assessing debonding in composite sandwich structures.

References

[1] Su, Z., and Ye, L. "Lamb wave-based quantitative identification of delamination in CF/EP composite structures using artificial neural algorithm". Composite Structures, 66(1-4): 627-637, 2004

[2] Seth, S. K., Spearing, S. M., and Constantinos, S. "Damage detection in composite materials using Lamb wave methods". Smart Materials and Structures, 11(2): 269-278, 2002

[3] Mustapha, S., Ye, L., Wang, D., and Lu, Y. "Assessment of debonding in sandwich CF/EP composite beams using A0 Lamb wave at low frequency". Composite Structures, 93(2): 483-491, 2011

[4] Qi, X., Rose, J. L., and Xu, C. "Ultrasonic guided wave nondestructive testing for helicopter rotor blades". 17th World Conference on Nondestructive Testing, Shanghai, China, 2008

[5] Song, F., Huang, G. L., and Hudson, K. "Guided wave propagation in honeycomb sandwich structures using a piezoelectric actuator/sensor system". Smart Materials and Structures, 18: 125007, 2009

[6] Mustapha, S., Ye, L., Wang, D., and Lu, Y. "Debonding detection in composite sandwich structures based on guided waves". Submitted to AIAA, 2004